Research Letter **DOI:** 10.15541/jim20240532

MnO_x/CeO_2-ZrO_2 Composite Oxides: Construction and Application in Soot Oxidation

LIU Panpan[1], YAO Peng[1], LIU Xuzi[1], QU Li[2], ZENG Lu[1], SONG Zhaohua[1], JIAO Yi[1], WANG Jianli[1,2], CHEN Yaoqiang[1,2]

(1. Institute of New Energy and Low-Carbon Technology, Sichuan University, Chengdu 610065, China; 2. College of Chemistry, Sichuan University, Chengdu 610065, China)

Abstract: Gasoline soot particles pose a severe threat to the ecological environment and human health, but they can be potentially filtered out by using catalytic gasoline particulate filter (cGPF), whose core component is a catalyst coating. To develop more effective catalyst coatings with excellent activity, stability, and water resistance, a kind of composite oxide MnO_x/CeO_2-ZrO_2 was synthesized using different methods, and its soot oxidation performance was evaluated under low O_2 concentrations. Herein, MnO_x/CeO_2-ZrO_2 prepared by impregnation (abbreviated as MCZ-IM) exhibits a T_{50} (temperature required for 50% soot conversion) of 329 ℃ in 1% O_2 and 370 ℃ in 0.5% O_2, displaying better comprehensive performance when compared to catalysts prepared by high-energy ball milling (abbreviated as MCZ-HB) and co-precipitation (abbreviated as MCZ-CP). Structure-activity relationship reveals that soot oxidation under low O_2 concentrations is weakly correlated with textural and structural properties, but strongly depends on the generation and migration of active oxygen species (AOS), especially superoxide (O_2^-) and peroxide (O_2^{2-}) anions, which are linked to redox properties, oxygen storage and release capacity, as well as amount of oxygen vacancies. The impregnation method enhances oxygen species adsorption, activation and desorption more effectively, endowing it with a more effective approach to enhancing AOS generation and mobility. Therefore, this study not only provides a preparation strategy for particulate matter oxidation catalysts applicable to actual operating conditions, but also offers insights into the migration of AOS at low O_2 concentrations.

Key words: MnO_x/CeO_2-ZrO_2; catalyst; soot; active oxygen species

Vehicles with gasoline direct injection (GDI) engines have gradually become a research hotspot due to their better combustion efficiency compared to port fuel injection (PFI) engines. However, a significant drawback of GDI engines is the generation of more fine particulate matter (PM) emissions. cGPF is considered an effective technology for purifying PM, capable of removing PM from GDI engines. Catalysts coated on the in-wall of cGPF can promote PM oxidation at lower temperature[1-3]. Therefore, there has been a significant interest in developing PM oxidation catalysts in recent years[1-10]. PM, as a common model for soot particles[5,11-14], poses a threat to the environment and human health[15-17]. Additionally, the low O_2 concentration, almost no NO_x and high temperature in gasoline exhaust present challenges[13, 18, 19]. Therefore, soot oxidation catalysts for gasoline exhaust must meet higher performance standards.

Since the 1980s, various catalysts with excellent soot oxidation activity have been used to remove diesel soot, including noble metal catalysts[6, 14, 20, 21], transition metal oxide catalysts[5, 13, 22], perovskite-like oxide catalysts[7, 12, 19, 23], and rare earth oxide catalysts[1, 24-27]. Among these, CeO_2-based catalysts are particularly promising for soot oxidation due to their excellent redox behavior and oxygen storage capacity (OSC)[25], with their relatively low cost making them more attractive. However, CeO_2 suffers from severe sintering and agglomeration under high-temperature exhaust gas from gasoline engines[28]. Incorporating zirconium oxide into CeO_2 to form solid solutions significantly improves thermal stability, OSC,

Received date: 2024-12-23; **Revised date:** 2025-04-19; **Published online:** 2025-05-09
Foundation item: Advanced Materials-National Science and Technology Major Project (2024ZD0606500); National Natural Science Foundation of China (21902110); Sichuan Provincial Science Foundation (2023NSFSC0093)
Biography: LIU Panpan (2000–), male, Master candidate. E-mail: liupanpan@stu.scu.edu.cn
刘盼盼(2000–), 男, 硕士研究生. E-mail: liupanpan@stu.scu.edu.cn
Corresponding author: JIAO Yi, associate professor. E-mail: jiaoyiscu@163.com
焦 毅, 副研究员. E-mail: jiaoyiscu@163.com

and AOS mobility[26, 29-30]. Moreover, Zr^{4+} addition creates structural defects, especially oxygen vacancies, which benefit the soot oxidation process[31]. Therefore, CeO_2-ZrO_2 catalysts exhibit better soot oxidation activity than pure CeO_2. Additionally, introducing manganese oxide (MnO_x) into CeO_2 forms MnO_x-CeO_2 based catalysts, which show excellent soot oxidation activity and low ignition temperature. This improvement is attributed to the multiple oxidation states of Mn and the high mobility of lattice oxygen[32-37]. However, while single oxide (CeO_2, MnO_x) and mixed oxides (MnO_x-CeO_2, CeO_2-ZrO_2) catalysts are highly effective for soot oxidation under sufficient oxidant conditions (at least 5% O_2 and/or 500–2000 μL/L NO_x in diesel exhaust)[24, 32-37], they still face significant challenges in gasoline exhaust atmospheres[13, 18-19]. Gasoline soot purification catalysts require better redox behavior, oxygen storage and release capacity, oxygen species adsorption, activation and desorption capacity, as well as more surface oxygen vacancies due to the oxygen-deficient environment.

Under the circumstances, developing an excellent catalyst that improves the redox behavior and OSC, and generates more AOS than MnO_x-CeO_2 and CeO_2-ZrO_2 is crucial. Incorporating a third metal oxide through effective doping is a promising strategy to enhance redox behavior and OSC. Zhao *et al*.[38] showed that ternary CeMnCu mixed oxides could lower the average valence state of Ce, promoting soot oxidation. In our previous work[29, 39], Y_2O_3 and La_2O_3 were introduced into CeO_2-ZrO_2, and MnO_x-doped CeO_2-ZrO_2 catalysts with different MnO_x contents were synthesized. The results demonstrated that MnO_x significantly improved redox behavior and soot oxidation activity[40]. However, while this doping method enhances redox performance and AOS migration, further investigation is required to address the lower oxygen concentration in gasoline engine exhaust.

The preparation method significantly influences the redox ability, OSC, AOS generation and migration, and thermal stability of Ce-based catalysts. In this study, MnO_x/CeO_2-ZrO_2 (MCZ) catalysts were synthesized *via* co-precipitation, impregnation, and high-energy ball milling, and their soot oxidation performance under stringent conditions was evaluated. The introduction of Mn species through different methods altered the structure, redox ability, and OSC of the catalysts, thereby affecting their catalytic activity. This study aims to identify the optimal MCZ catalyst for soot oxidation and evaluate the effect of loading methods on MnO_x distribution and catalytic performance.

1 Experimental

MCZ composite oxides were synthesized through co-precipitation[40-42], impregnation and high-energy ball milling methods, respectively, which were named as MCZ-CP, MCZ-IM and MCZ-HB.

The detailed preparation and characterization procedures, as well as test method of catalytic activity, are described in the supporting materials S1-S3.

2 Results and discussion

2.1 Catalyst performance

The soot conversion and CO_x concentration profiles of CZ, MCZ-CP, MCZ-IM, and MCZ-HB catalysts are shown in Fig. 1(a, b) and Fig. S1, while Fig. 1(c) displays T_{50} and T_{90} under different O_2 concentrations. The results demonstrated that MnO_x modification significantly promoted soot oxidation under both atmospheric conditions, with a more pronounced enhancement under high oxygen concentration (1.0% O_2), which may be due to the differences in textural and structural properties, redox ability, oxygen storage and release capacity, and amount of AOS. Notably, MCZ-IM exhibited the highest catalytic activity (T_{50} = 329 ℃, 1.0% O_2), surpassing previously reported Ce/Mn-based catalysts in other studies (Table S1).

Fig. 2(a) shows the variation trends of soot conversion during the four cycles of soot-TPO tests with 1.0% O_2. The soot conversion of MCZ-IM catalyst remained stable during the first three cycles, indicating excellent soot oxidation performance. However, T_{50} and T_{90} shifted to higher temperatures, and the catalytic activity decreased slightly in the fourth cycle, which may be due to catalyst loss during repeated grinding and/or aggregation of manganese species on the CZ surface[43].

Previous studies[4, 6, 44] have demonstrated that the introduction of NO is beneficial for the production of NO_2 intermediate, exhibiting a stronger oxidative capacity on soot than O_2. The soot conversions under various gas compositions with O_2 (0.5%/1.0%), O_2 (0.5%/1.0%) + NO (600 μL/L) and O_2 (0.5%/1.0%) + NO (600 μL/L) + H_2O (5%) in N_2 are shown in Fig. 2(b, c). NO (600 μL/L) incorporation has a negligible influence on soot oxidation in O_2 atmosphere, which is attributed to the insufficient O_2 concentration, high flow rate, and limited contact time in the cGPF. Additionally, due to the coverage of active sites by H_2O molecules below 300 ℃, the catalytic activity of MCZ-IM catalyst decreases slightly after the introduction of 5% H_2O[45]. On the whole, MCZ-IM exhibits excellent activity, stability, and modest anti-water property during soot oxidation in the simulated gasoline engine exhaust.

2.2 Textural-structural properties, microstructure and surface element composition

Table 1 summarizes textural properties of CZ and

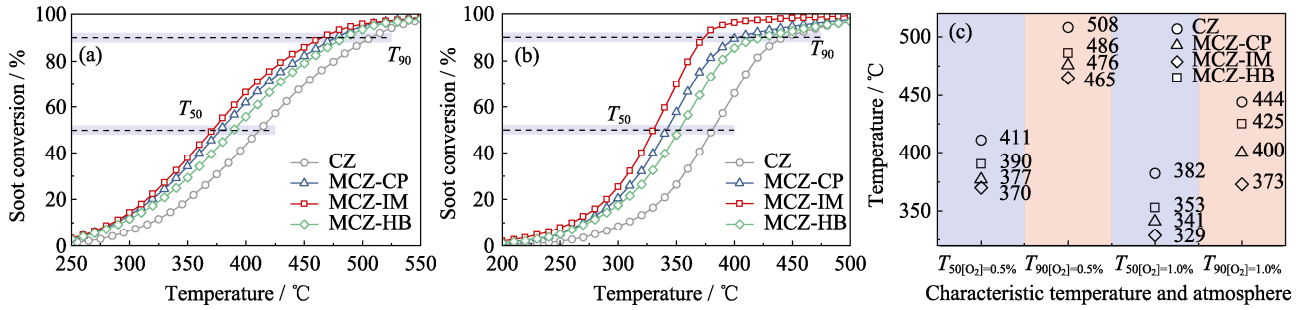

Fig. 1 Soot conversion, T_{50}, and T_{90} of the catalysts under different oxygen concentrations with reaction conditions of flow rate at 500 mL/min and N_2 balance
(a, b) Soot conversion under (a) 0.5% and (b) 1.0% O_2; (c) T_{50} and T_{90} under different oxygen concentrations

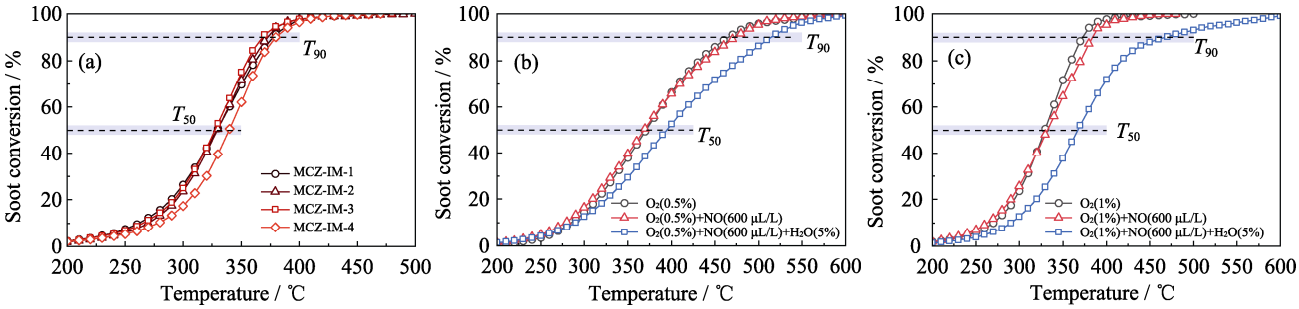

Fig. 2 Catalytic stability under 1.0% O_2 (a) and effects of NO and H_2O on catalytic activity of MCZ-IM catalyst with different atmospheres (b, c)

Table 1 Textural and structural properties of the prepared catalysts

Sample	Surface area[a] /($m^2 \cdot g^{-1}$)	Pore volume[a] /($mL \cdot g^{-1}$)	Mean pore diameter[a] /nm	Crystallinity[b] /%	Grain size[c] /nm
CZ	110.3	0.26	9.40	52.1	7.2
MCZ-CP	145.9	0.34	9.64	40.2	5.1
MCZ-IM	79.2	0.22	11.30	45.6	7.4
MCZ-HB	81.3	0.22	10.80	44.8	7.6

[a] Determined by N_2 adsorption-desorption; [b] Obtained by XRD; [c] Obtained by applying the Scherrer formula to the (111) peak of XRD

MCZ catalysts. MCZ-CP exhibits larger specific surface area (145.9 m^2/g) and pore volume (0.34 mL/g) than those of the other catalysts, which is related to reduced grain size. Specifically, the smaller grain size, the greater number of grain boundaries. These additional grain boundaries may be exposed on the particle surfaces, forming more pores or increasing surface roughness of particles, which results in enhanced specific surface area and pore volume. However, the specific surface areas exhibit a sharp reduction after doping with MnO_x using the impregnation method and high-energy ball milling method, possibly due to surface rearrangement, pore plugging, or homogenization between MnO_x and CeO_2-ZrO_2. Interestingly, the trend in surface area of the catalysts is not positively correlated with soot conversion.

XRD patterns are presented in Fig. 3(a). All samples mainly consist of $Ce_{0.4}Zr_{0.6}O_2$ solid solution with characteristic peaks at 2θ=29.2°, 33.8°, 48.4°, and 58.1° (JCPDS 38-1439). No peaks associated with MnO_x species are detected in MCZ-CP and MCZ-IM, indicating MnO_x are amorphous or well dispersed within the framework of CZ. Weak Mn_2O_3 peaks in MCZ-HB sample suggest that Mn doping by high-energy ball milling method limits the interaction between MnO_x and CZ. Moreover, the intensities of diffraction peaks of MCZ catalysts decrease compared with those of CZ, especially for MCZ-CP, indicating a decrease in the crystallinity of MCZ. Notably, MCZ-CP exhibits the smallest grain size, whereas the other samples have similar grain sizes. This difference is attributed to the inherent characteristics of co-precipitation method. Thus, no significant relationship is observed between the XRD results and soot oxidation activity.

In addition, the particle size of MnO_x varies with the preparation method. Considering previous study[40], XRD data, and the characteristics of the preparation methods, the relative order of MnO_x particle sizes in different MCZ samples is inferred to be MCZ-HB>MCZ-IM>MCZ-CP.

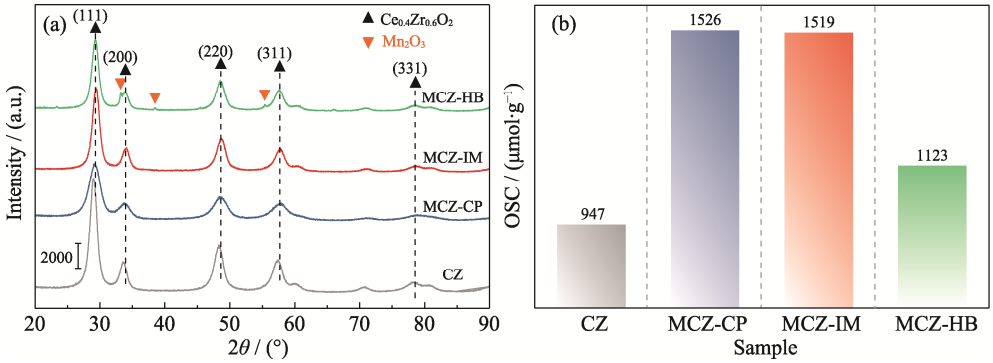

Fig. 3　XRD patterns (a) and OSC results (b) of the catalysts

However, no clear correlation is observed between this order and catalytic activity.

SEM-EDS results are presented in Fig. 4 and Table 2. The three samples have no significant differences in microstructure. The surface element contents obtained by EDS analysis from three different locations in the same sample are shown in Table S2. The surface O contents of MCZ-CP and MCZ-IM are larger than MCZ-HB, suggesting that MnO_x loading by co-precipitation and impregnation methods can produce more surface O, which contributes to soot oxidation. The surface Mn

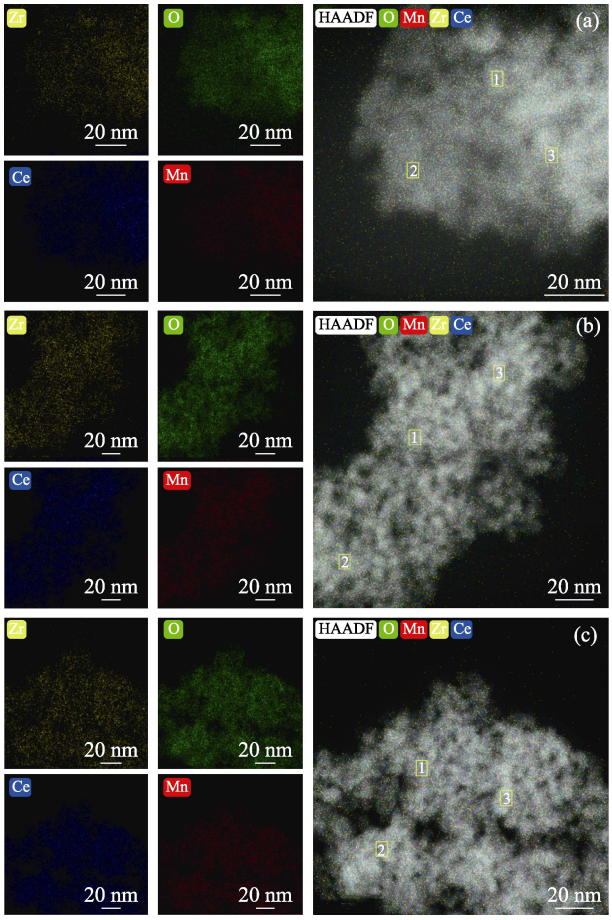

Fig. 4　Microstructure and surface elements of MCZ-CP (a), MCZ-IM (b) and MCZ-HB (c) catalysts

Table 2　Surface elements composition of the catalysts

Sample	Mass fraction/%			
	O	Mn	Zr	Ce
MCZ-CP	24.38	2.98	22.44	50.20
MCZ-IM	24.13	7.54	23.14	45.18
MCZ-HB	21.52	1.03	24.58	52.87

introduced *via* impregnation method is much higher than that *via* the other methods, which can enhance the concentration of active sites on the surface and improve the contact efficiency between soot and these active sites. Consequently, a higher number of active species can easily migrate to the gas-solid-solid three-phase interface and react with soot, aligning with the catalytic performance observed in soot oxidation.

2.3　Redox properties and oxygen storage capacity

The redox abilities influencing soot oxidation activity were evaluated using H_2-TPR (Fig. 5(a)). Previous studies[6, 28, 44] showed that two distinct types of cerium species in CeO_2 are reducible. The first type is the reduction of surface Ce^{4+} ions, peaking in the temperature range of 450–550 ℃, whereas the second type involves reduction of bulk Ce^{4+} ions, with peak temperatures occurring at approximately 800 ℃. Obviously, a single broad reduction peak was detected for CZ sample in the range of 350–630 ℃, which is attributed to the co-reduction of surface and bulk cerium oxides because the doped Zr integrated into the lattice of CeO_2[41]. Notably, two distinct reduction peaks can be observed in MCZ-IM and MCZ-HB samples. The first peak at 247/335 ℃ belongs to the reduction of MnO_2/Mn_2O_3 to Mn_3O_4, while the second peak at 351/433 ℃ is associated with concurrent reduction of Ce^{4+} to Ce^{3+} and Mn_3O_4 to MnO[37]. For MCZ-CP sample, a single broad reduction peak is discernible, potentially due to the strong interaction between MnO_x and CZ. Furthermore, the reduction peaks of MCZ-IM shift to a lower

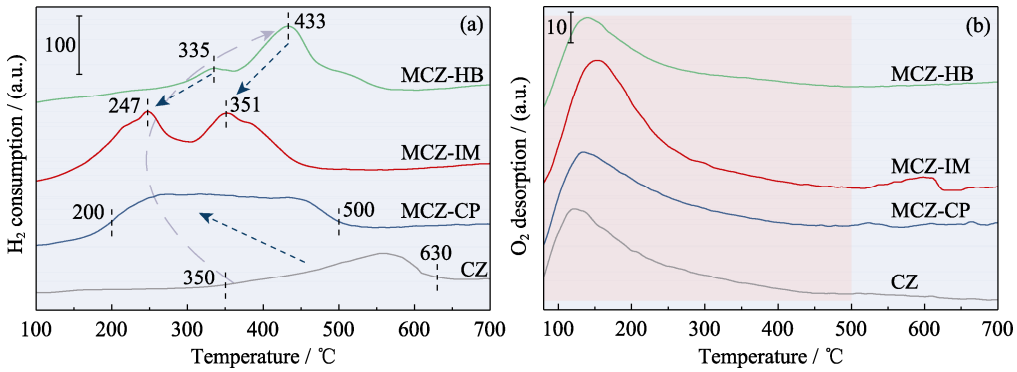

Fig. 5 H_2-TPR (a) and O_2-TPD (b) profiles of the catalysts

temperature compared with those of MCZ-CP, MCZ-HB and CZ samples, indicating that the incorporation of MnO_x *via* impregnation method significantly enhances the reducibility of CZ, thereby facilitating the reduction process by surface modification. In summary, the MCZ-IM sample exhibits the best reducibility at a low temperature.

O_2-TPD analysis was used to evaluate O_2 adsorption-desorption capacity and identify types of oxygen species during desorption (Fig. 5(b)). Each sample presents a broad desorption peak ranging from 80 to 500 ℃, corresponding to the desorption of both surface adsorbed and lattice oxygen species[32, 37]. Notably, the peak intensities of MCZ-IM and MCZ-CP are stronger than that of CZ, suggesting that MnO_x doping significantly enhances the amount of desorbed oxygen species and adsorption-desorption capacity for oxygen species. The desorption of oxygen species mainly occurs at low temperature (below 500 ℃), which is more suitable for soot oxidation. Moreover, the OSC results of the catalysts obtained by O_2 pulse injection method are shown in Fig. 3(b). The MCZ samples demonstrate higher OSC values than CZ sample, and MCZ-IM and MCZ-CP present a significant advantage among these catalysts. A higher OSC value enables catalysts to maximize O_2 usage and is typically associated with more oxygen vacancies, which can enhance soot oxidation performance. However, the OSC value of MCZ-CP with lower soot oxidation activity is similar to that of MCZ-IM, indicating that some oxygen species do not participate in the soot oxidation reaction, which is attributed to the poor contact efficiency between the soot and oxygen species in MCZ-CP sample with a lower amount of surface MnO_x.

2.4 Surface oxygen vacancies and active oxygen species

The surface oxygen vacancies and chemical states of surface elements were characterized by Raman spectra (Fig. 6(a)). All samples display three strong vibrational peaks at 465, 620 and 1208 cm^{-1}, corresponding to the characteristic peaks of F_{2g} type from the CeO_2 fluorite-like structure, interstitial oxygen vacancies and second-order longitudinal optical (2LO) mode[43, 46]. Moreover, F_{2g} and 2LO peaks exhibit slight changes after the doping with MnO_x by different methods compared with CZ. The peak corresponding to interstitial oxygen vacancies is significantly enhanced with the introduction of MnO_x, particularly through co-precipitation and impregnation methods. In addition, the ratio of peak area at 620 cm^{-1} to that at 465 cm^{-1} (A_{620}/A_{465}) is used to reflect relative oxygen vacancies concentration[37, 43, 47]. The oxygen vacancies concentration is elevated with MnO_x doping by co-precipitation and impregnation methods, which is beneficial for soot oxidation through the improved lattice oxygen mobility and adsorption and activation of gas phase oxygen.

The surface elemental status was investigated by XPS (Fig. 6(b-d)). For Ce3d spectra, $Ce3d_{3/2}$ and $Ce3d_{5/2}$ peaks were marked as V and U, respectively. The peaks labeled as V, V_2, V_3 and U, U_2, U_3 are assigned to $Ce^{4+}3d_{3/2}$ and $Ce^{4+}3d_{5/2}$, respectively. While the peaks labeled as V_1 and U_1 belong to $Ce^{3+}3d_{3/2}$ and $Ce^{3+}3d_{5/2}$, respectively. For Mn2p spectra, the binding energies at 641.1 and 642.8 eV are attributed to Mn^{3+} (or Mn^{2+}) and Mn^{4+}, respectively.

Surface elemental relative concentrations were determined by calculating the ratio of peak area of Ce^{3+} or Ce^{4+} (Mn^{4+}) to total peak area of Ce (Mn) species, with the results presented in Table 3. Notably, Mn doping increases the surface Ce^{4+} concentration, and the value of Mn^{4+} reaches the highest in MCZ-IM and Ce^{4+} also reaches a higher value. Mn^{4+} and Ce^{4+} can produce more interstitial oxygen vacancies, which facilitate the generation of surface AOS and play important roles in soot oxidation[47]. Therefore, the higher values of Mn^{4+} and Ce^{4+} in MCZ-IM are responsible for its excellent activity, aligning with studies reporting that introducing

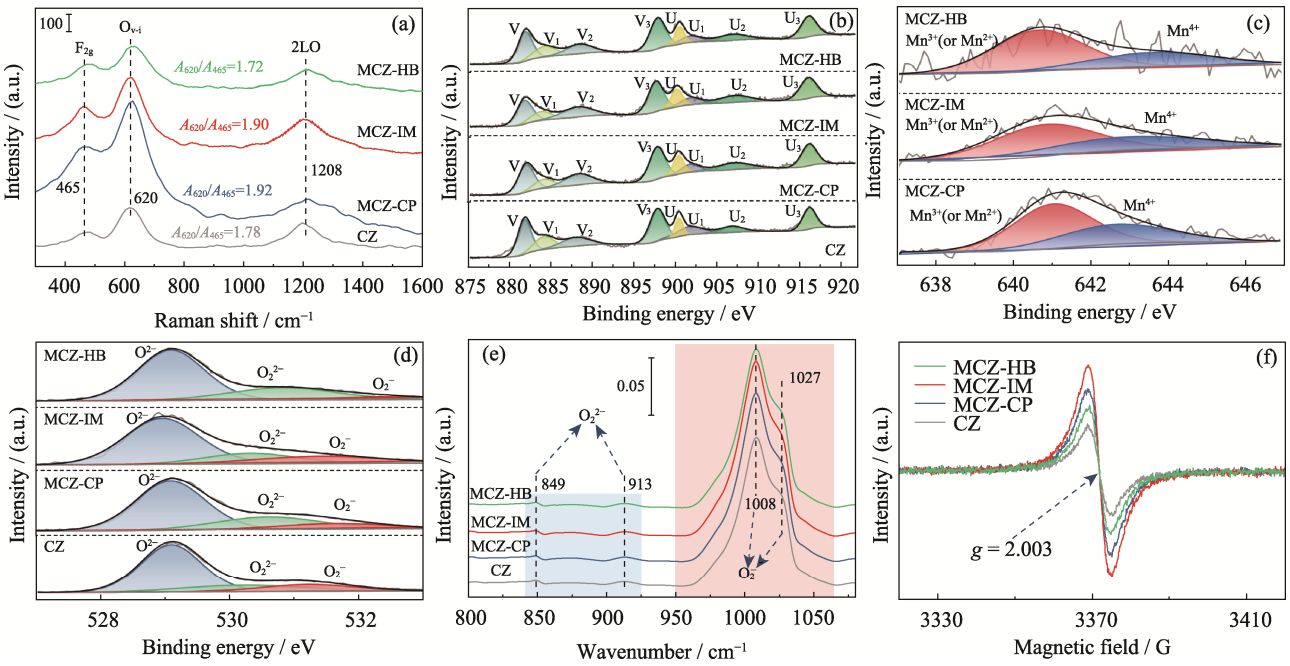

Fig. 6　Surface oxygen vacancies and active oxygen species of the samples
(a) Raman spectra; (b-d) Ce3d (b), Mn2p (c), and O1s (d) XPS spectra; (e) DRIFTS spectra of O_2 adsorption collected at 300 ℃; (f) Low-temperature EPR. Colorful figures are available on website

Table 3　Surface compositions and charge states of Ce, Mn and O species derived from XPS analysis

Catalyst	Ce^{3+}/Ce	Ce^{4+}/Ce	Mn^{4+}/Mn	$(O_2^{2-}+O_2^-)/O_T$	O_2^-/O_T
CZ	0.21	0.79	—	0.28	0.09
MCZ-CP	0.14	0.86	0.36	0.35	0.11
MCZ-IM	0.15	0.85	0.39	0.34	0.17
MCZ-HB	0.17	0.83	0.32	0.31	0.06

extraneous elements can promote lattice oxygen mobility and be beneficial for the activation of oxygen species[47-48].

As illustrated in Fig. 6(d), each sample displays three O1s characteristic peaks. The initial peak in the range of 528.6–529.7 eV is associated with surface lattice oxygen species (O^{2-}), the second peak in the range of 529.5–531.0 eV corresponds to O_2^{2-}, and the third peak in the range of 530.8–532.5 eV is ascribed to O_2^-[6, 28], which enhances the mobility of oxygen species and promotes soot oxidation. $(O_2^{2-}+O_2^-)/O_T$ (where $O_T = O^{2-} + O_2^{2-} + O_2^-$) and O_2^-/O_T are used to reflect the relative concentrations of AOS (Table 3). The relative concentration of AOS (O_2^{2-} and O_2^-) increases with MnO_x doping, especially when using the impregnation method, which results in a higher AOS concentration. The increase of active O_2^- species in MCZ-IM also has a close relationship with the highest activity among these MCZ catalysts. Furthermore, DRIFTS spectra of O_2 adsorption collected at 300 ℃ (Fig. 6(e)) indicate that AOS (O_2^- and O_2^{2-}) are generated[46, 49-50]. In addition, EPR results (Fig. 6(f)) show a symmetrical resonance signal peak at g of 2.003, serving as a characteristic peak for oxygen vacancies. Its intensity is proportional to the oxygen vacancy concentration[51-52]. The concentration order is MCZ-IM>MCZ-CP>MCZ-HB>CZ, matching the catalytic activity trend. Therefore, the formation and migration of AOS and the amount of oxygen vacancies are two important factors that affect soot oxidation.

2.5　Key factors for soot oxidation

The varying soot oxidation performance of the MCZ catalysts can be ascribed to two primary factors. One is the contact efficiency between reactants (soot and O_2) and catalysts[20], which affects the migration distance of AOS. A shorter distance results in higher migration efficiency and greater availability of AOS. The other is the intrinsic properties of catalysts, including textural and structural properties, microtopography, redox ability, AOS adsorption-desorption capacity, oxygen storage-release capacity, and amount of surface oxygen vacancies. Since all catalyst evaluations were conducted under the same contact conditions and O_2 content, the differences

in activity among the three MCZ catalysts are mainly due to their intrinsic properties.

Fig. 7 illustrates the key factors influencing soot oxidation in this study. EDS analysis reveals that different doping methods lead to variations in surface element distribution (especially Mn), fundamentally altering the catalyst properties. N_2 adsorption-desorption and XRD results indicate that textural and structural properties are not directly correlated with catalytic performance. While some studies[12, 53] suggest that specific surface area significantly impacts soot oxidation, MCZ-IM and MCZ-HB have much smaller surface areas than MCZ-CP, yet MCZ-IM exhibits superior catalytic activity. In addition, low-temperature reducibility is crucial for soot oxidation, as it reflects the generation rate of AOS, according to the Mars-van Krevelen mechanism. The superior low-temperature reducibility of MCZ-IM is closely linked to its enhanced soot oxidation performance. Furthermore, variations in catalytic activity among these samples correlate with O_2 desorption behavior below 500 ℃[32]. The amount of AOS and surface oxygen vacancies significantly affect AOS mobility. Notably, the most active species, Mn^{4+}, Ce^{4+}, and AOS, play a role in soot oxidation comparable to that of surface oxygen vacancies, as evidenced by Raman, EPR, and XPS data. At the microscopic level, oxygen vacancies serve as active sites for AOS generation and as carriers for their migration. However, excessive oxygen vacancies may cause the transformation of O_2^- into O_2^{2-} and O^{2-} during migration, while insufficient vacancies can limit AOS generation. In conclusion, AOS generation and migration are essential for soot oxidation. MnO_x addition *via* the impregnation method proves to be an effective strategy for enhancing both processes, likely due to the efficient utilization of MnO_x.

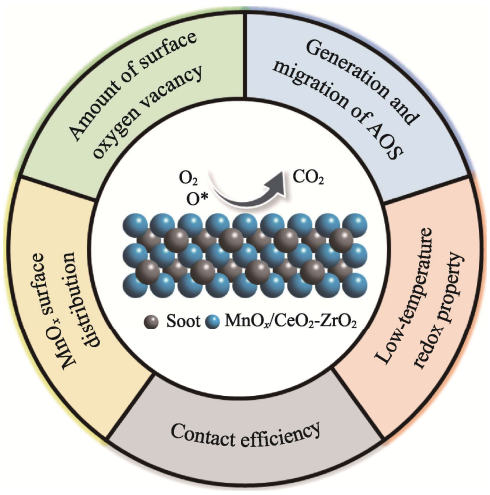

Fig. 7 Key factors for soot oxidation in this study

3 Conclusions

In this study, MCZ-IM exhibits superior activity for soot oxidation, with a T_{50} value of 329 ℃ in 1% O_2. The structure-activity relationship reveals that properties related to the generation and migration of AOS, including redox ability, AOS adsorption-desorption capacity, oxygen storage-release capacity, and the amount of surface oxygen vacancies, as well as the contact efficiency between soot and catalysts, are enhanced by MnO_x doping *via* the impregnation method. An intimate relationship exists between AOS generation and migration and soot oxidation under harsh conditions, and the impregnation-based MnO_x doping is recognized as an effective strategy to optimize MnO_x utilization. Thus, surface modification methods (such as impregnation) may be more effective in improving catalytic activity than bulk modification methods (such as co-precipitation) for gas-solid-solid reactions (such as soot oxidation). This enhancement can be attributed to improved accessibility of active sites to soot, which significantly increases AOS migration efficiency toward the soot surface, thereby facilitating the oxidation process.

Supporting materials

Supporting materials related to this article can be found at https://doi.org/10.15541/jim20240532.

References:

[1] LIU S, FANG Z, WU X. CeO_2-based materials for gasoline soot combustion: reaction mechanism and catalyst design. *Journal of the Chinese Society of Rare Earths*, 2022, **40(3):** 351.

[2] LIU S, WU X D, TANG J, *et al*. An exploration of soot oxidation over CeO_2-ZrO_2 nanocubes: do more surface oxygen vacancies benefit the reaction? *Catalysis Today*, 2017, **281:** 454.

[3] MATARRESE R. Catalytic materials for gasoline particulate filters soot oxidation. *Catalysts*, 2021, **11(8):** 890.

[4] ZHAO M J, DENG J L, LIU J, *et al*. Roles of surface-active oxygen species on 3DOM cobalt-based spinel catalysts $M_xCo_{3-x}O_4$ (M=Zn and Ni) for NO_x-assisted soot oxidation. *ACS Catalysis*, 2019, **9(8):** 7548.

[5] WANG X, JIN B F, FENG R X, *et al*. A robust core-shell silver soot oxidation catalyst driven by Co_3O_4: effect of tandem oxygen delivery and Co_3O_4-CeO_2 synergy. *Applied Catalysis B*: *Environmental*, 2019, **250:** 132.

[6] LI Y F, QIN T, WEI Y C, *et al*. A single site ruthenium catalyst for robust soot oxidation without platinum or palladium. *Nature Communications*, 2023, **14:** 7149.

[7] YU D, WANG L Y, ZHANG C L, *et al*. Alkali metals and cerium-modified La–co-based perovskite catalysts: facile synthesis, excellent catalytic performance, and reaction mechanisms for soot combustion. *ACS Catalysis*, 2022, **12(24):** 15056.

[8] LIU S R, LUO S T, WU X D, *et al*. Application of silica-alumina as hydrothermally stable supports for Pt catalysts for acid-assisted

soot oxidation. *Rare Metals*, 2023, **42(5):** 1614.

[9] YU X H, REN Y, YU D, *et al*. Hierarchical porous K-OMS-2/3DOM-m $Ti_{0.7}Si_{0.3}O_2$ catalysts for soot combustion: easy preparation, high catalytic activity, and good resistance to H_2O and SO_2. *ACS Catalysis*, 2021, **11(9):** 5554.

[10] ZHU C X, DU S C, WANG S B, *et al*. PGM-free metal oxide nanoarray forests for water-promoted low-temperature soot oxidation. *Applied Catalysis B*: *Environmental*, 2024, **341:** 123336.

[11] JIN B F, ZHAO B H, LIU S, *et al*. $SmMn_2O_5$ catalysts modified with silver for soot oxidation: dispersion of silver and distortion of mullite. *Applied Catalysis B*: *Environmental*, 2020, **273:** 119058.

[12] LIU J X, YANG Z, ZHAI Y J, *et al*. High performance of $PrMnO_3$ perovskite catalysts for low-temperature soot oxidation. *Separation and Purification Technology*, 2025, **354:** 129227.

[13] YANG W N, WANG S M, LI K Z, *et al*. Highly selective α-Mn_2O_3 catalyst for cGPF soot oxidation: surface activated oxygen enhancement *via* selective dissolution. *Chemical Engineering Journal*, 2019, **364:** 448.

[14] ZHAO Z, MA J, LI M, *et al*. Model Ag/CeO_2 catalysts for soot combustion: roles of silver species and catalyst stability. *Chemical Engineering Journal*, 2022, **430:** 132802.

[15] AWAD O I, MA X, KAMIL M, *et al*. Particulate emissions from gasoline direct injection engines: a review of how current emission regulations are being met by automobile manufacturers. *Science of the Total Environment*, 2020, **718:** 137302.

[16] WANG X C, CHEN W H, HUANG Y H, *et al*. Advances in soot particles from gasoline direct injection engines: a focus on physical and chemical characterisation. *Chemosphere*, 2023, **311:** 137181.

[17] KONTSES A, TRIANTAFYLLOPOULOS G, NTZIACHRISTOS L, *et al*. Particle number (PN) emissions from gasoline, diesel, LPG, CNG and hybrid-electric light-duty vehicles under real-world driving conditions. *Atmospheric Environment*, 2020, **222:** 117126.

[18] NOSSOVA L, CARAVAGGIO G. Effect of dopants on soot oxidation over doped Ag/ZrO_2 catalysts for catalyzed gasoline particulate filter. *Catalysis Communications*, 2023, **182:** 106744.

[19] HERNÁNDEZ W Y, LOPEZ-GONZALEZ D, NTAIS S, *et al*. Silver-modified manganite and ferrite perovskites for catalyzed gasoline particulate filters. *Applied Catalysis B*: *Environmental*, 2018, **226:** 202.

[20] YAO P, HUANG Y, JIAO Y, *et al*. Soot oxidation over Pt-loaded CeO_2-ZrO_2 catalysts under gasoline exhaust conditions: soot-catalyst contact efficiency and Pt chemical state. *Fuel*, 2023, **334:** 126782.

[21] KUBO H, OHSHIMA Y, KATO S, *et al*. The effect of supported metal Species on soot oxidation over PGM/CeO_2-ZrO_2. *Bulletin of the Chemical Society of Japan*, 2024, **97(10):** uoae092.

[22] LUO J B, ZHU X B, ZHONG Z W, *et al*. Enhanced catalytic soot oxidation over co-based metal oxides: effects of transition metal doping. *Molecules*, 2023, **29(1):** 41.

[23] ZHANG P, MEI X L, ZHAO X C, *et al*. Boosting catalytic purification of soot particles over double perovskite-type $La_{2-x}K_xNiCoO_6$ catalysts with an ordered macroporous structure. *Environmental Science & Technology*, 2021, **55(16):** 11245.

[24] XIONG J X, ZHANG B J, LIANG Z F, *et al*. Highly reactive peroxide species promoted soot oxidation over an ordered macroporous $Ce_{0.8}Zr_{0.2}O_2$ integrated catalyzed diesel particulate filter. *Environmental Science & Technology*, 2024, **58(18):** 8096.

[25] HE J S, YAO P, QIU J, *et al*. Enhancement effect of oxygen mobility over $Ce_{0.5}Zr_{0.5}O_2$ catalysts doped by multivalent metal oxides for soot combustion. *Fuel*, 2021, **286:** 119359.

[26] DENG J, LI S S, XIONG L, *et al*. Preparation of nanostructured CeO_2-ZrO_2-based materials with stabilized surface area and their catalysis in soot oxidation. *Applied Surface Science*, 2020, **505:** 144301.

[27] WANG L M, ZHAO N R, YIN X Y, *et al*. Highlights on the key roles of interfaces between CeO_2-based oxide and perovskite ($LaMnO_3$/LaFeO3) in creating active oxygen species for soot oxidation. *Fuel*, 2024, **356:** 129444.

[28] ZHENG C L, MAO D J, XU Z Y, *et al*. Strong Ru-CeO_2 interaction boosts catalytic activity and stability of Ru supported on CeO_2 nanocube for soot oxidation. *Journal of Catalysis*, 2022, **411:** 122.

[29] XIONG L, YAO P, LIU S, *et al*. Soot oxidation over CeO_2-ZrO_2 based catalysts: the influence of external surface and low-temperature reducibility. *Molecular Catalysis*, 2019, **467:** 16.

[30] MISHRA U K, CHANDEL V S, SINGH O P, *et al*. Synthesis of CeO_2 and Zr-doped CeO_2 ($Ce_{1-x}Zr_xO_2$) catalyst by green synthesis for soot oxidation activity. *Arabian Journal for Science and Engineering*, 2023, **48(1):** 771.

[31] LIU S, WU X D, WENG D, *et al*. Ceria-based catalysts for soot oxidation: a review. *Journal of Rare Earths*, 2015, **33(6):** 567.

[32] LI Y F, QIN T, XIONG J, *et al*. Mn-modified near-surface atomic structure of CeO_2 nanorods for promoting catalytic oxidation of auto-exhaust carbon particles. *Chemical Engineering Science*, 2023, **282:** 119309.

[33] ZHAO H, ZHOU X X, WANG M, *et al*. Highly active MnO_x–CeO_2 catalyst for diesel soot combustion. *RSC Advances*, 2017, **7(6):** 3233.

[34] ALINEZHADCHAMAZKETI A, KHODADADI A A, MORTAZAVI Y, *et al*. Catalytic evaluation of promoted CeO_2-ZrO_2 by transition, alkali, and alkaline-earth metal oxides for diesel soot oxidation. *Journal of Environmental Sciences*, 2013, **25(12):** 2498.

[35] XING L L, YANG Y X, CAO C M, *et al*. Decorating CeO_2 nanoparticles on Mn_2O_3 nanosheets to improve catalytic soot combustion. *ACS Sustainable Chemistry & Engineering*, 2018, **6(12):** 16544.

[36] YANG Y, FANG J, MENG Z W, *et al*. Catalytic activity and influence factors of Mn-Ce mixed oxides by hydrothermal method on diesel soot combustion. *Molecular Catalysis*, 2022, **524:** 112334.

[37] SUN Y, FANG S Y, XU J C, *et al*. Unveiling the surface chemical reactions during multi-phase catalytic oxidation of soot on nanoengineering/interfacing/doping-prepared Mn-CeO_2 catalysts using TG-MS and operando DRIFTS-MS. *Langmuir*, 2023, **39(44):** 15773.

[38] ZHAO H, LI H C, PAN Z F, *et al*. Design of CeMnCu ternary mixed oxides as soot combustion catalysts based on optimized Ce/Mn and Mn/Cu ratios in binary mixed oxides. *Applied Catalysis B*: *Environmental*, 2020, **268:** 118422.

[39] LI S S, DENG J, WANG J L, *et al*. Effects of thermal treatment conditions on redox properties of ceria-zirconia materials. *Journal of Rare Earths*, 2023, **41(12):** 1969.

[40] YAO P, HE J S, JIANG X, *et al*. Factors determining gasoline soot abatement over CeO_2–ZrO_2-MnO_x catalysts under low oxygen concentration condition. *Journal of the Energy Institute*, 2020, **93(2):** 774.

[41] ZHANG H L, WANG J L, ZHANG Y H, *et al*. A study on H_2-TPR of $Pt/Ce_{0.27}Zr_{0.73}O_2$ and $Pt/Ce_{0.27}Zr_{0.70}La_{0.03}O_x$ for soot oxidation. *Applied Surface Science*, 2016, **377:** 48.

[42] WANG S N, WANG J L, HUA W B, *et al*. Designed synthesis of Zr-based ceria–zirconia–neodymia composite with high thermal stability and its enhanced catalytic performance for Rh-only three-way catalyst. *Catalysis Science & Technology*, 2016, **6(20):** 7437.

[43] HE H, LIN X T, LI S J, *et al*. The key surface species and oxygen vacancies in MnO_x(0.4)-CeO_2 toward repeated soot oxidation. *Applied Catalysis B*: *Environmental*, 2018, **223:** 134.

[44] WANG H L, LUO S T, ZHANG M S, *et al*. Roles of oxygen

vacancy and O_x^- in oxidation reactions over CeO_2 and Ag/CeO_2 nanorod model catalysts. *Journal of Catalysis*, 2018, **368:** 365.

[45] XIONG J, WU Q Q, MEI X L, *et al*. Fabrication of spinel-type $Pd_xCo_{3-x}O_4$ binary active sites on 3D ordered meso-macroporous Ce-Zr-O_2 with enhanced activity for catalytic soot oxidation. *ACS Catalysis*, 2018, **8(9):** 7915.

[46] KHATUN R, PAL R S, SHOEB M A, *et al*. Generation of active oxygen species by CO_2 dissociation over defect-rich Ni-Pt/CeO_2 catalyst for boosting methane activation in low-temperature dry reforming: experimental and theoretical study. *Applied Catalysis B*: *Environmental*, 2024, **340:** 123243.

[47] LIN X T, LI S J, HE H, *et al*. Evolution of oxygen vacancies in MnO_x-CeO_2 mixed oxides for soot oxidation. *Applied Catalysis B*: *Environmental*, 2018, **223:** 91.

[48] ZHANG Z R, KANG R N, YI X K, *et al*. Migration roles of different oxygen species over Cu/CeO_2 for propane and soot combustion. *Separation and Purification Technology*, 2024, **349:** 127820.

[49] XU J W, ZHANG Y, XU X L, *et al*. Constructing $La_2B_2O_7$ (B = Ti, Zr, Ce) compounds with three typical crystalline phases for the oxidative coupling of methane: the effect of phase structures, superoxide anions, and alkalinity on the reactivity. *ACS Catalysis*, 2019, **9(5):** 4030.

[50] SUBBOTINA I R, BARSUKOV D V. Direct evidence of the key role of UV-formed peroxide species in photocatalytic gas–solid oxidation in air on anatase TiO_2 particles. *Physical Chemistry Chemical Physics*, 2020, **22(4):** 2200.

[51] ZHANG M Y, DUAN X L, GAO Y, *et al*. Tuning oxygen vacancies in oxides by configurational entropy. *ACS Applied Materials & Interfaces*, 2023, **15(39):** 45774.

[52] MAO H F, XU M L, LI S J, *et al*. Accelerating surface lattice oxygen activation of Pt/TiO_{2-x} by modulating the interface electron interaction for efficient photocatalytic toluene oxidation. *ACS ES&T Engineering*, 2023, **3(11):** 1851.

[53] LOU D M, SONG G F, XU K W, *et al*. The oxidation performance of a carbon soot catalyst based on the Pt-Pd synergy effect. *Energies*, 2024, **17(7):** 1737.

MnO_x/CeO_2-ZrO_2 复合氧化物的构筑及其在碳烟氧化中的应用

刘盼盼[1], 姚 鹏[1], 刘栩孜[1], 屈 丽[2], 曾 路[1],
宋兆华[1], 焦 毅[1], 王健礼[1,2], 陈耀强[1,2]

(四川大学 1. 新能源与低碳技术研究院; 2. 化学学院, 成都 610065)

摘 要: 汽油机尾气碳烟颗粒严重威胁着生态环境和人类健康, 而催化型汽油颗粒物过滤器(cGPF)是一种有效的净化技术, 其核心为催化剂涂层。本研究采用不同制备方法构筑了 MnO_x/CeO_2-ZrO_2 复合氧化物, 在低 O_2 浓度下考察了其碳烟氧化性能, 旨在开发具有卓越催化活性、稳定性以及抗水性的碳烟氧化催化剂涂层。结果表明, 通过浸渍法制备的 MnO_x/CeO_2-ZrO_2(MCZ-IM)在 1% O_2 中, 其 T_{50}(碳烟转化率达 50%所需的温度)为 329 ℃; 在 0.5% O_2 中, 其 T_{50} 为 370 ℃。相较于高能球磨法(MCZ-HB)和共沉淀法(MCZ-CP)制备的催化剂, MCZ-IM 展现出更优的综合性能。构效关系表明, 低 O_2 浓度下碳烟氧化性能与催化剂的织构和结构性质呈弱相关, 而与活性氧物种(AOS)——超氧(O_2^-)和过氧(O_2^{2-})阴离子的生成及迁移密切相关, 其中涉及氧化还原性能、储释氧能力以及氧空位数量。MCZ-IM 在氧物种的吸附、活化和脱附方面更具优势, 因此浸渍法被认为是提高 AOS 生成和迁移的更优方法。本研究不仅提供了一种适用于实际运行条件下颗粒物(PM)氧化催化剂的制备策略, 而且深入揭示了低 O_2 浓度环境中 AOS 的迁移机制。

关 键 词: MnO_x/CeO_2-ZrO_2; 催化剂; 碳烟; 活性氧物种

中图分类号: O643 **文献标志码:** A **文章编号:** 1000-324X(2025)11-1300-09

Supporting Materials:

MnO_x/CeO_2-ZrO_2 Composite Oxides: Construction and Application in Soot Oxidation

LIU Panpan[1], YAO Peng[1], LIU Xuzi[1], QU Li[2], ZENG Lu[1], SONG Zhaohua[1], JIAO Yi[1], WANG Jianli[1,2], CHEN Yaoqiang[1,2]

(1. Institute of New Energy and Low-Carbon Technology, Sichuan University, Chengdu 610065, China; 2. College of Chemistry, Sichuan University, Chengdu 610065, China)

S1 Catalysts preparation

MCZ composite oxides were synthesized through co-precipitation, impregnation and high-energy ball milling methods, respectively. In the three MCZ catalysts, a mass fraction of CeO_2-ZrO_2 was 90% with a Ce/Zr molar ratio of 4:6, and a mass fraction of MnO_x calculated based on MnO_2 was 10%. All the catalysts were calcined at 600 ℃ for 3 h in static air.

Firstly, CeO_2-ZrO_2, MnO_x and MCZ composite oxides were synthesized by the co-precipitation method, which is similar to that in our previous works[S1-S3], and denoted as CZ, M, and MCZ-CP, respectively. Then, the as-prepared CZ (9 g) and M (1 g) were mixed together by high-energy ball milling for 3 min, and the product was denoted as MCZ-HB. Finally, 10% (in mass) MnO_x, using $Mn(NO_3)_2$ aqueous solution (a mass fraction of 50%) as precursor, was introduced into the above CZ by incipient wetness impregnation, and it was denoted as MCZ-IM.

S2 Catalysts characterization

The catalysts were characterized by N_2 adsorption-desorption, X-ray diffraction (XRD), hydrogen temperature programmed reduction (H_2-TPR), oxygen storage capacity (OSC), oxygen temperature programmed desorption (O_2-TPD), Raman spectra, X-ray photoelectron spectroscopy (XPS) and scanning transmission electron microscopy-energy dispersive spectroscopy (SEM-EDS) according to the procedure described in our previous works[S1, S3]. Diffuse reflectance infrared fourier transform spectroscopy (DRIFTS) was conducted on a spectrometer (INVENIO-S, Bruker, USA). The powder was loaded into a reaction cell with a KBr window, and a total gas flow rate was maintained at 100 mL/min. The sample was heated to 450 ℃ at a rate of 20 ℃/min and activated in He for 1 h. Then, the temperature decreased to 300 ℃, and the background spectrum was collected. Finally, the sample was exposed to oxygen for 30 min, and the spectrum was collected. Oxygen vacancies were characterized by low-temperature electron paramagnetic resonance (EPR) spectrometer (Bruker A300, Bruker, USA) at –196 ℃ with a frequency of 9.45 GHz and a power supply of 20.03 mW, and the *g* value was determined from the frequency and magnetic field strength.

S3 Test method of catalytic activity

Special black 6 (Orion) was used as a model compound of soot with a mean particle size of 17 nm, a surface area of 300 m^2/g, and a volatile organic compounds (VOCs) content of 18%. The as-prepared catalysts and soot (100 mg : 10 mg) were ground carefully in an agate mortar for 5 min, and then 100 mg SiC powder was added to prevent reaction runaway. The soot oxidation activities of catalysts were evaluated through temperature programmed oxidation (TPO) method.

The obtained sample was deposited on a porous disc within a 12 mm diameter quartz reaction tube, and quartz cotton was placed on both sides of the sample. A gas mixture of 0.5% or 1% O_2/N_2 at a flow rate of 500 mL/min was passed through the catalyst bed while heating from room temperature to 700 ℃ at a rate of 5 ℃/min. In addition, cycle test and different gas compositions were used to study the stability and the effects of NO and H_2O on the soot oxidation activity. During the soot-TPO process, CO_x emissions were continuously detected by a gas chromatograph (GC9790 Ⅱ, Fuli) equipped with a methanator and a flame ionization detector (FID) using 99.999% N_2 as a carrier gas. The soot-TPO curve was integrated, and the ratio of partial peak area ($A_{partial}$) to total peak area (A_{total}) was used to evaluate soot conversion (Equation (1)). The catalytic performance was evaluated based on T_{50} and T_{90} parameters, which denote the temperatures required for achieving 50% and 90% soot conversions, respectively.

$$\text{Conversion} = \frac{A_{\text{partial}}}{A_{\text{total}}} \times 100\% \quad (1)$$

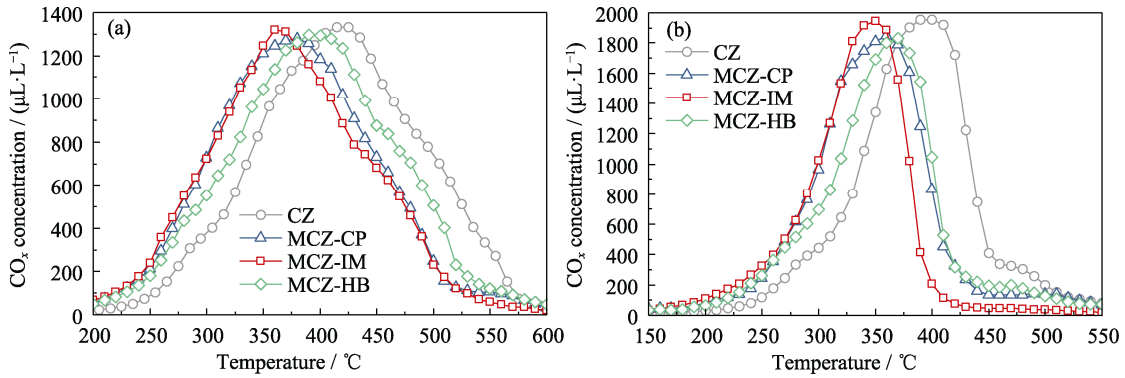

Fig. S1 Generated CO_x concentration of soot oxidation over the catalysts

Reaction conditions: flow rate at 500 mL/min and N_2 balance; [O_2]: (a) 0.5% and (b) 1.0%

Table S1 Comparison of catalytic activity with other studies

Catalyst	Method	Reaction condition (gas and flow rate)	Heating rate/ (℃·min^{-1})	Catalyst and soot mass ratio	Contact mode	T_{50}/T_{max}/ ℃	Ref.
MCZ-IM	Incipient wetness impregnation	1% O_2 0.5% O_2 (500 mL/min)	5	10 : 1	Tight	329 370	This work
M10-CZ	Co-precipitation	0.5% O_2 (500 mL/min)	5	10 : 1	Loose	520	[S1]
Mn_2O_3	Flame spray pyrolysis	1% O_2 + 2% H_2O (500 mL/min)	3.3	15 : 1	Tight	321	[S4]
10LM-CZ	Co-precipitation and citric acid complexation impregnation	1% O_2 (100 mL/min)	5	10 : 1	Tight	362	[S5]
0.57Mn-CeO_2	Nitrate aerosol pyrolysis	10% O_2 (100 mL/min)	10	4 : 1	Tight	355	[S6]
5 Mn-CP	Solution combustion synthesis	Air (100 mL/min)	10	10 : 1	Tight	365	[S7]
CM5	EDTA–Citrate	Air (100 mL/min)	10	10 : 1	Tight	360	[S8]
$Ce_{0.5}Mn_{0.5}O_2$	Sol–gel	12% O_2 (100 mL/min)	15	4 : 1	Tight	383	[S9]
CMO_st	Solvothermal	–	10	19 : 1	Tight	442	[S10]
CM	Co-precipitation	Air (100 mL/min)	10	4 : 1	Tight	396	[S11]
CMC	Co-precipitation	Air (100 mL/min)	–	4 : 1	Tight	363	[S12]
$Ce_{0.9}Mn_{0.1}$	Solid-phase grinding	10% O_2 (50 mL/min)	10	10 : 1	Tight	389	[S13]
Mn-Fib Ce	Plasma-assisted deposition	18% O_2 + 0.1%NO (20 mL/min)	5	20 : 1	Tight	384	[S14]

Table S2 Surface elements composition of the prepared catalysts

Sample	Element	Atomic fraction/%				Mass fraction/%			
		Area 1	Area 2	Area 3	Average	Area 1	Area 2	Area 3	Average
MCZ-CP	O	62.48	66.22	69.82	66.17	21.55	24.14	27.45	24.38
	Mn	2.49	2.85	2.92	2.75	2.52	3.06	3.37	2.98
	Zr	15.70	11.73	10.37	12.60	26.47	20.91	19.94	22.44
	Ce	19.33	19.20	16.89	18.47	49.45	51.90	49.24	50.20
MCZ-IM	O	60.16	63.95	68.43	64.18	21.21	24.43	26.76	24.13
	Mn	6.91	8.73	4.92	6.86	7.16	9.81	5.66	7.54
	Zr	16.25	12.07	9.86	12.73	28.02	22.54	18.86	23.14
	Ce	16.68	15.25	16.80	16.24	43.61	43.22	48.72	45.18
MCZ-HB	O	61.05	65.04	63.64	63.24	20.63	22.36	21.58	21.52
	Mn	0.89	0.91	1.30	1.03	0.88	0.92	1.30	1.03
	Zr	19.84	11.62	12.91	14.79	32.79	19.54	21.41	24.58
	Ce	18.23	22.43	22.15	20.94	45.70	57.19	55.71	52.87

References:

[S1] YAO P, HE J S, JIANG X, *et al*. Factors determining gasoline soot abatement over CeO_2-ZrO_2-MnO_x catalysts under low oxygen concentration condition. *Journal of the Energy Institute*, 2020, **93(2):** 774.

[S2] ZHANG H L, WANG J L, ZHANG Y H, *et al*. A study on H_2-TPR of Pt/$Ce_{0.27}Zr_{0.73}O_2$ and Pt/$Ce_{0.27}Zr_{0.70}La_{0.03}O_x$ for soot oxidation. *Applied Surface Science*, 2016, **377:** 48.

[S3] WANG S N, WANG J L, HUA W B, *et al*. Designed synthesis of Zr-based ceria-zirconia-neodymia composite with high thermal stability and its enhanced catalytic performance for Rh-only three-way catalyst. *Catalysis Science & Technology*, 2016, **6(20):** 7437.

[S4] SINGER C, HAHN C, PHAN D Q, *et al*. Oxidation of soot in gasoline exhaust on Mn_2O_3 catalyst. *Applied Catalysis A*: *General*, 2023, **663:** 119316.

[S5] WANG L M, ZHAO N R, YIN X Y, *et al*. Highlights on the key roles of interfaces between CeO_2-based oxide and perovskite ($LaMnO_3$/LaFeO3) in creating active oxygen species for soot oxidation. *Fuel*, 2024, **356:** 129444.

[S6] SUN Y, FANG S Y, XU J C, *et al*. Unveiling the surface chemical reactions during multi-phase catalytic oxidation of soot on nanoengineering/interfacing/doping-prepared Mn-CeO_2 catalysts using TG-MS and operando DRIFTS-MS. *Langmuir*, 2023, **39(44):** 15773.

[S7] PATIL S S, DASARI H P, SHIRASANGI R, *et al*. Diesel soot oxidation over Mn-Pr-Ce oxide catalysts: structural changes and the impact of Mn doping. *Materials Advances*, 2025, **6(3):** 1131.

[S8] SHOURYA A, DASARI H P. Manganese doped Ceria ($Ce_{1-x}Mn_xO_{2-\delta}$ (x = 0–0.3)) catalysts synthesized by EDTA-Citrate method for soot oxidation activity. *Chemical Papers*, 2022, **76(11):** 7095.

[S9] HUANG H, LIU J H, SUN P, *et al*. Effects of Mn-doped ceria oxygen-storage material on oxidation activity of diesel soot. *RSC Advances*, 2017, **7(12):** 7406.

[S10] DOROFEEVA N V, SAVEL'EVA A S, GRABCHENKO M V, *et al*. Ce-Zr-Mn oxide catalysts for soot combustion: the role of preparation method. *The Journal of Physical Chemistry C*, 2024, **128(32):** 13432.

[S11] MUKHERJEE D, VENKATASWAMY P, DEVAIAH D, *et al*. Crucial role of titanium dioxide support in soot oxidation catalysis of manganese doped ceria. *Catalysis Science & Technology*, 2017, **7(14):** 3045.

[S12] GOVINDA RAO B, JAMPAIAH D D, VENKATASWAMY D P, *et al*. Enhanced catalytic performance of manganese and cobalt co-doped CeO_2 catalysts for diesel soot oxidation. *ChemistrySelect*, 2016, **1(21):** 6681.

[S13] ZHOU B, XI K, FAN L J, *et al*. A comparative study on Ce-Pr and Ce-Mn mixed oxide catalysts toward soot catalytic combustion. *Applied Catalysis A*: *General*, 2018, **562:** 1.

[S14] RODRIGUEZ M, LEONARDI S A, HANON F, *et al*. Plasma-assisted deposition of Mn and Fe phases on CeO_2 biomorphic fibers for soot combustion and CO oxidation. *Catalysis Today*, 2024, **431:** 114457.